Coupling regularizes individual units in noisy populations

Cheng Ly* and G. Bard Ermentrout†
Department of Mathematics, University of Pittsburgh, 139 University Place, Pittsburgh, PA 15260
(Received 6 October 2009; revised manuscript received 13 November 2009; published 21 January 2010)

The regularity of a noisy system can modulate in various ways. It is well known that coupling in a population can lower the variability of the entire *network*; the collective activity is more regular. Here, we show that diffusive (reciprocal) coupling of two simple Ornstein-Uhlenbeck (O-U) processes can regularize the *individual*, even when it is coupled to a noisier process. In cellular networks, the regularity of individual cells is important when a select few play a significant role. The regularizing effect of coupling surprisingly applies also to general nonlinear noisy oscillators. However, unlike with the O-U process, coupling-induced regularity is robust to different kinds of coupling. With two coupled noisy oscillators, we derive an asymptotic formula assuming weak noise and coupling for the variance of the period (i.e., spike times) that accurately captures this effect. Moreover, we find that reciprocal coupling can regularize the individual period of higher dimensional oscillators such as the Morris-Lecar and Brusselator models, even when coupled to noisier oscillators. Coupling can have a counterintuitive and beneficial effect on noisy systems. These results have implications for the role of connectivity with noisy oscillators and the modulation of variability of individual oscillators.

DOI: 10.1103/PhysRevE.81.011911 PACS number(s): 87.18.Tt, 05.45.Xt, 84.35.+i, 87.18.Sn

I. INTRODUCTION

The underlying dynamics of how stochastic cellular networks behave in the presence of stimuli are complicated. For example, in neural networks signals are transmitted with high fidelity in the presence of many stochastic forces [1]. How is this achieved? The variability of activity and its modulation is studied here to gain a better understanding of network dynamics.

It is known that inhibitory synaptic coupling can decrease the variance of the spike times of a population of neurons, and increase the signal-to-noise ratio [2,3]. Reduction in spike time variability of a large population of oscillators (integrate-and-fire model) has been observed with excitatory coupling [4] and with state dependent (multiplicative) noise [5]. Coupling in populations of pancreatic beta cells [6] and cardiac cells [7] leads to regular activity even though the individual cells behave stochastically. The large network that produces regular circadian rhythms consists of individual molecular processes (formation/binding of proteins, transcription of genes, etc.) that are stochastic [8]. However, in all of these studies, a decrease in individual cell (oscillator) variability due to coupling was not studied, but rather only the variability of the network. A small number of cells can drive most of the network activity in various biological systems. This is known, for example, in the thalamus [9], the heart [10], and in central pattern generators for respiration and locomotion [11]. Also, very few neurons encode sensory stimuli in rat somatosensory cortex [12] and in auditory sounds [13]. Hence, regularity at the individual level may have important consequences in cellular networks.

We first explore the effect of coupling on the regularity of a simple linear system of diffusively coupled Ornstein-Uhlenbeck (O-U) processes. A straight forward calculation shows that reciprocal coupling results in more regular behavior. Also, coupling to noisier units can surprisingly lower the variability of both (the less noisier and noisier process). Next, we focus on coupled oscillators because they have been effectively utilized by many scientists to describe phenomena in diverse fields ranging from the physical to the biological sciences [14–17]. Including the effects of noise (thermal-dynamic, molecular biological processes, heterogeneity, etc.) to account for a larger class of systems has attracted considerable attention [18]. We find the results for the O-U processes hold for nonlinear noisy oscillators as well. However, with noisy oscillators, the reduction in variability is robust to many types of coupling. Thus, coupling in noisy oscillators is beneficial when regularity is required.

In the context of coupled noisy oscillators, the full probability density of the random period is difficult to compute analytically and numerically. Thus, we derive an asymptotic approximation assuming weak noise and weak coupling that captures the observed phenomena. Also, we find the results hold for networks of higher dimensional systems such as Morris-Lecar cells and Brusselators.

II. DIFFUSIVELY COUPLED ORNSTEIN-UHLENBECK PROCESSES

Consider a system of N diffusively coupled O-U processes with 0 mean ($\langle X_j \rangle = 0$),

$$\dot{X}_j = -X_j + \sigma_j \xi_j(t) + \frac{K}{N-1} \sum_i (X_i - X_j), \tag{1}$$

for $j = 1, \ldots, N$, $\xi_j(t)$ are independent white noise processes: $\langle \xi_j(t) \rangle = 0$, $\langle \xi_j(t) \xi_i(t) \rangle = \delta_{ij} \delta(t - t')$, where $\delta_{ij} = 1$ if $i = j$ and 0 if $i \neq j$. As the coupling strength $K \geq 0$ increases, the $X_j(t)$'s become more synchronous. For $N \gg 1$, its not surprising that the (steady-state) variance of the individual processes, X_1 without loss of generality, decreases with coupling. Briefly, this can be understood by defining $Y := \frac{1}{N} \Sigma_{j=1}^{N} X_j$, which

*chengly@math.pitt.edu
†bard@math.pitt.edu

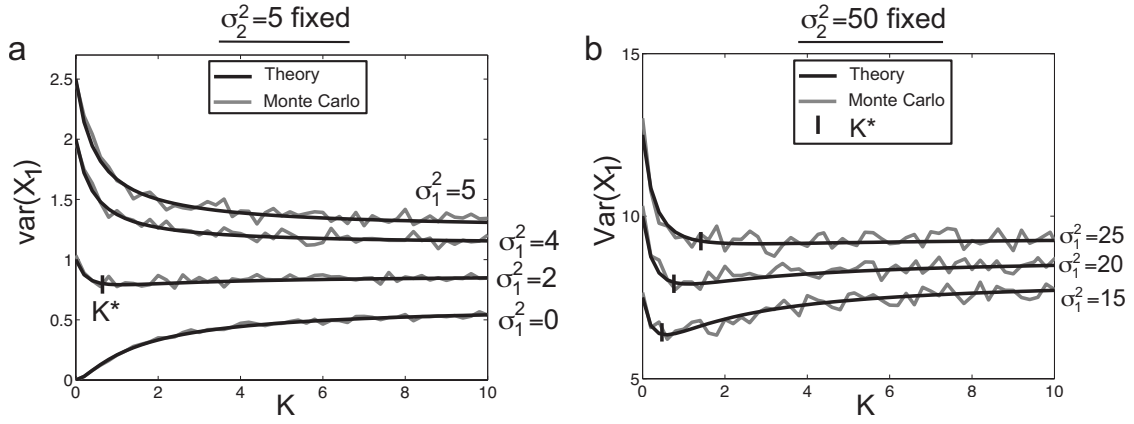

FIG. 1. Coupling effects on the regularity of an individual O-U process. (a) var(X_1) is plotted for $\sigma_2^2=5$ fixed, and $\sigma_1^1=0,2,4,5$. Simulations (gray) match the theory [black, Eq. (2)]. $K^*=\frac{1+\sqrt{3}}{5}$ for $\sigma_1^2=2$. (b) Similar to (a) except $\sigma_2^2=50$ fixed and $\sigma_1^2=15,20,25$. As σ_1 decreases, K^* decreases for a fixed value of σ_2^2.

evolves according to: $\dot{Y}=-Y+\bar{\sigma}\xi(t)$, where $\bar{\sigma}=\frac{1}{N}\sqrt{\Sigma_{j=1}^N\sigma_j^2}$. The steady-state density of Y is a Gaussian with 0 mean and variance $\bar{\sigma}^2$. The equation for X_1 is can be rewritten as: $\dot{X}_1=-X_1+\sigma_1\xi_1(t)+\frac{KN}{N-1}(Y-X_1)$. Intuitively, larger K synchronizes X_1 with Y, which has smaller variance for large N, leading to a decrease in variance of X_1. This argument depends on $N\to\infty$; we show that this also holds for small N even if the noise amplitudes greatly differ. Consider $N=2$. In this case, the joint steady-state density is a multivariate Gaussian and can be calculated analytically via the steady-state Fokker-Planck equation; this involves algebraic equations for the coefficients. We do not report the calculations but only give the results. The variance of X_1 is

$$\mathrm{var}(X_1)=\frac{1}{4}\frac{K^2(\sigma_1^2+\sigma_2^2)+\sigma_1^2(4K+2)}{2K^2+3K+1}. \tag{2}$$

If $\sigma_1>\sigma_2>0$, one can verify that var(X_1) decreases monotonically for all $K>0$; coupling to less noisier X_2 only regularizes X_1 (compared to uncoupled), which is not surprising. For $0<\sigma_1\leq\sigma_2$, a straight forward calculation gives $K^*=\frac{\sigma_2^2-3\sigma_1^2-\sqrt{\sigma_2^2-\sigma_1^2}}{5\sigma_1^2-3\sigma_2^2}$ as the critical coupling value. We see that coupling regularizes X_1 for all $K>0$ as long as $\sigma_1^2>\frac{3}{5}\sigma_2^2$. Thus, coupling with a (possibly) *noisier* X_2 regularizes X_1 as long as σ_2 is not too big. If $\sigma_1^2<\frac{3}{5}\sigma_2^2$ and the numerator of K^* is negative, then coupling decreases var(X_1) until K^*, after which var(X_1) will increase. As $K\to\infty$, $\mathrm{var}(X_1)\to\frac{1}{4}\frac{\sigma_1^2+\sigma_2^2}{2}$. These results are highlighted in Fig. 1. If $\sigma_2\gg\sigma_1$, coupling leads to an increase in var(X_1)$>\sigma_1^2$ (not shown). As $\frac{\sigma_2}{\sigma_1}\to\infty$, K^* approaches a negative value; thus, all $K>0$ leads an increase in var(X_1). This can be achieved for finite $\frac{\sigma_2}{\sigma_1}$. Of course, if the coupling is not diffusive (e.g., $K<0$), var(X_1) can dramatically increase.

III. NOISY OSCILLATOR MODEL

In the same vein as the O-U processes, we study the variability of coupled nonlinear noisy oscillators. We outline a phase reduction technique of high dimensional noisy oscillators to obtain a simple yet general model that captures the qualitative dynamics. The reduced model [Eqs. (8) and (9) below] are also amenable to analysis.

Consider two identically coupled noisy oscillators of the form

$$\dot{X}_1=F(X_1)+\tilde{K}G(X_1,X_2)+\tilde{\sigma}_1\Xi_1(t), \tag{3}$$

$$\dot{X}_2=F(X_2)+\tilde{K}G(X_2,X_1)+\tilde{\sigma}_2\Xi_2(t), \tag{4}$$

where $X_j\in\mathbb{R}^n$, Ξ_j is an n vector of independent (componentwise) white noise processes. In the absence of noise ($\tilde{\sigma}_j=0$) and coupling ($\tilde{K}=0$), the system $\dot{X}_j=F(X_j)$ has an asymptotically stable limit cycle $X_0(t)=X_0(t+\tau)$, with period τ. The statistics of the random times T that it takes for the oscillators to complete a cycle with noise and coupling is the central focus. In neural models, these are the spike times, i.e., when voltage variable reaches its maximum. Concrete examples of Eqs. (3) and (4) will be studied in Sec. V.

We assume Eqs. (3) and (4) are stochastic differential equations of the Itô type, so that care must be taken when changing variables. Assume X_j is only reciprocally coupled to X_i. There is a function $\phi:\mathbb{R}^n\to S^1$ mapping a neighborhood of the limit cycle to the phase on a circle, $\theta\in[0,\tau)$. Defining $\theta_j=\phi(X_j)$, we see that θ_j satisfies:

$$\frac{d\theta_j}{dt}=1+\nabla_X\phi(X_j)\cdot[\tilde{K}G(X_j,X_i)+\tilde{\sigma}_j\Xi_j(t)]. \tag{5}$$

This equation is exact, but not useful since we do not know X_j or X_i. Assuming small perturbations, we can approximate X_j by $X_0(\theta_j)$ (the limit cycle) to obtain an equation for θ_j,

$$\dot{\theta}_j\approx 1+\tilde{K}Z(\theta_j)\cdot G[X_0(\theta_j),X_0(\theta_i)]+\tilde{\sigma}_jZ(\theta_j)\cdot\Xi_j(t), \tag{6}$$

where $Z(\theta):=\nabla_X\phi[X_0(\theta)]$. The function, $Z(\theta)$ is called the adjoint and satisfies the linear equation

$$Z'(\theta)=-D_XF[X_0(\theta)]^TZ(\theta). \tag{7}$$

The method of averaging is applied to the coupling term, so that it can be replaced by the coupling function $H(\theta_i-\theta_j)=\frac{1}{\tau}\int_0^\tau Z(t)\cdot G\{X_0(t),X_0[t+(\theta_i-\theta_j)]\}dt$ (see Kuramoto

[14]). If coupling and noise only occurs in the first variable, which is often the case with many oscillators, then the components of the G and $\Xi_j(t)$ are zero except for the first component. In $Z(\theta)$, we call the first component $\Delta(\theta)$. $\Delta(\theta)$ is proportional to the *phase resetting curve* or PRC of the neuron or oscillator, a quantity which is experimentally measurable. Assume the period is 1 without loss of generality. It is important to note that with a white noise process $\Xi_j(t)$, the mapping to θ_j requires additional care. We can consider $\Xi_j(t)$ as a limit of smooth functions and pass to appropriate limits after the mapping. This can be rigorously justified [19,20]. To obtain an SDE in the Itô sense, we use Itô lemma. The result is

$$\dot{\theta}_1 = 1 + KH(\theta_2 - \theta_1) + \frac{\sigma_1^2}{2}\Delta'(\theta_1)\Delta(\theta_1) + \sigma_1\Delta(\theta_1)\xi_1(t), \tag{8}$$

$$\dot{\theta}_2 = 1 + KH(\theta_1 - \theta_2) + \frac{\sigma_2^2}{2}\Delta'(\theta_2)\Delta(\theta_2) + \sigma_2\Delta(\theta_2)\xi_2(t), \tag{9}$$

where $\Delta(\theta)$ is the infinitesimal phase-resetting curve (PRC), H is the coupling function, $\theta_j \in [0,1)$ is the phase that resets to 0 when equal to 1, and $\xi_j(t)$ are independent white noise processes: $\langle \xi_j(t)\rangle = 0$, $\langle \xi_j(t)\xi_i(t)\rangle = \delta_{ij}\delta(t-t')$, where $\delta_{ij}=1$ if $i=j$ and 0 if $i \neq j$. A detailed discussion of the phase reduction of noisy oscillators can be found in [21].

Recall that we are interested in the statistics of the period T rather than the phase of the oscillator in contrast to the O-U processes in the last section. Monte Carlo simulations were performed to study the variability of the period, var(T), as coupling K varies. We considered the two canonical type-I ($\Delta_\beta = 1-\cos(2\pi\theta)$) and type-II [$\Delta_\alpha = -\sin(2\pi\theta)$] PRCs [22], set $\sigma_1 = \sigma_2$, and considered various coupling functions: $H=-\sin(2\pi\psi)$ antiphase coupling [for θ_1, Eq. (8)], $H=\sin(2\pi\psi)$ synchronous coupling, and $H=-\sin(4\pi\psi)$ [where $\psi = \frac{1}{4}, \frac{3}{4}$ are the stable phase differences in the absence of noise]. Simulations show that coupling always decreases var(T) of θ_1 compared to $K=0$ (Fig. 2), independent of the coupling function. The magnitudes of var(T) seem small, but note that the phase model is in normalized units and perturbations are small. The reduction in variability is appreciable in full oscillator models (Sec. V). To analyze this behavior, we derive an asymptotic theory for var(T) assuming weak noise and weak coupling (calculations in Appendix A).

IV. ASYMPTOTIC THEORY FOR STATISTICS OF THE PERIOD OF A PHASE MODEL

The full probability density function of the random crossing times $\theta_1(T)=1$ cannot be obtained analytically, and is difficult to compute numerically via the Fokker-Planck equation [23]. even in this simplified model (see Appendix B). We thus characterize T by its mean $\langle T\rangle$ and variance var(T). In order to better understand the observed phenomena, we rely on asymptotic methods to obtain an approximate formula for var(T) assuming $\sigma = O(\varepsilon)$ and $K = O(\varepsilon)$. Detailed

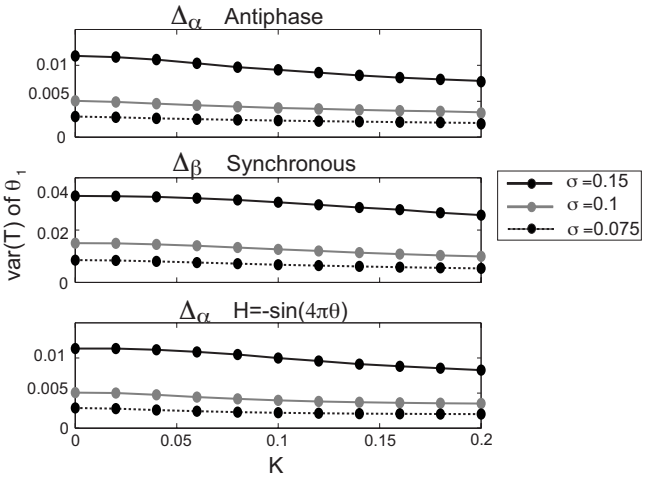

FIG. 2. Coupling reduces variability of phase models when $\sigma_1=\sigma_2$. Monte Carlo simulations show for many coupling functions and (small) noise levels that coupling regularizes the individual oscillator. a) $H=-\sin(2\pi\psi)$ antiphase coupling with $\Delta_\alpha=-\sin(2\pi\theta)$. (b) $H=\sin(2\pi\psi)$ synchronous coupling with $\Delta_\beta=1-\cos(2\pi\theta)$. (c) $H=\sin(-4\pi\psi)$ so $\psi=\frac{1}{4},\frac{3}{4}$ are stable states without noise and with Δ_α.

calculations are given in Appendix A. The formula is [cf. Eqs. (A33)–(A38)],

$$\mathrm{var}(T) = c_1(\sigma_1)^2 + c_2(\sigma_1)^2K + c_3(\sigma_1K)^2 + c_4(\sigma_2K)^2 + c_5(\sigma_1)^4 + O(\varepsilon^5), \tag{10}$$

where the coefficients c_j of each depend on Δ, H, and the steady-state distribution of the phase difference $\psi=\theta_2-\theta_1$ (mod 1), which we denote by $p(\psi)$.

In general, Eq. (10) has to be computed numerically, but it is straight forward to do so. For the canonical Δ's, we see that the lowest order coupling term $c_2(\sigma_1)^2K$ has a coefficient that is negative for a large class of coupling functions, consistent with the observed decrease in variance. The coefficient c_2 is proportional to

$$-\int_0^1 [H'(\psi) + 3H(\psi)]p(\psi)d\psi$$

for both $\Delta_\alpha=-\sin(2\pi\theta)$ and $\Delta_\beta=1-\cos(2\pi\theta)$. This term is negative because the stable states determined by H (i.e., stable in the absence of noise) has positive $H'(\psi_0)$ values *with* $p(\psi_0)$ sharply peaked; at the unstable states, $H'<0$ where the p values are small [Fig. 3(a)-i with antiphase coupling and Δ_α; Fig. 3(a)-ii with synchronous coupling and Δ_β]. From the figure, we see that the term $3H(\psi)$ slightly shifts the peak where $H'(\psi_0)$ is maximal i.e., H' has larger magnitude than $3H$ (gray curve). Integrating against the density of phase differences, $p(\psi)$ (black curve), weights the positive peaks of $H'+3H$ more favorably than the negative troughs, resulting in a decrease of var(T) with $0<K\ll 1$. This explanation is applicable to many coupling functions H in the asymptotic regime.

The asymptotic theory [Eq. (10)] is compared with Monte Carlo simulations for the two PRCs $\Delta_\alpha=-\sin(2\pi\theta)$ [Fig. 3(b)-i] and $\Delta_\beta=1-\cos(2\pi\theta)$ [Fig. 3(b)-ii] with equal

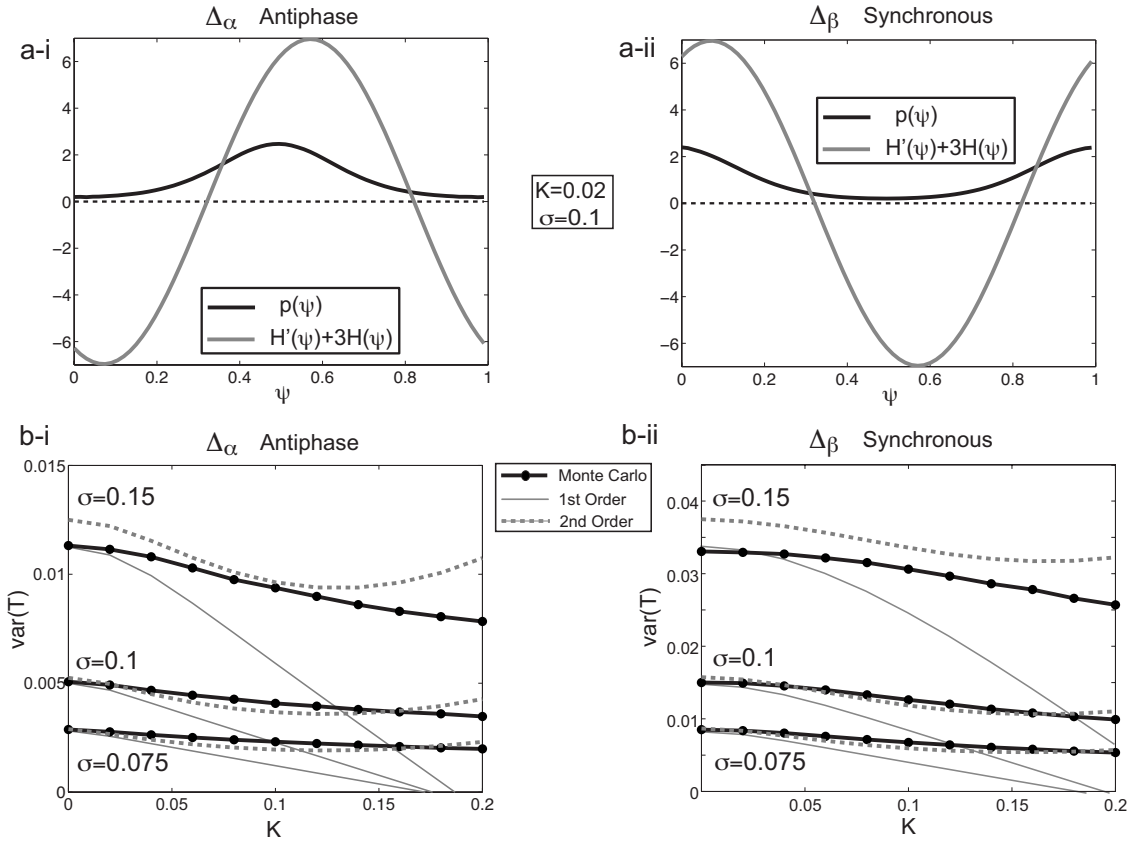

FIG. 3. Decrease in variability with coupling. (a) The dominant term with small coupling $-\int_0^1[H'(\psi)+3H(\psi)]p(\psi)d\psi$ is negative for synchronous [(a)-i] and antiphase coupling [(a)-ii] with the two canonical PRCs: $\Delta_\alpha=-\sin(2\pi\theta)$ and $\Delta_\beta=1-\cos(2\pi\theta)$, respectively. $\psi=\theta_2-\theta_1$ (mod 1), $K=0.02$, $\sigma_1=\sigma_2=0.1$. (b) Monte Carlo simulations of the variance of T for different coupling values K qualitatively matches the asymptotic theory [Eq. (10)] for small parameters ($\sigma_1=\sigma_2$). [(b)-i] Δ_α with antiphase coupling $H=-\sin(2\pi\psi)$ (in θ_1). [(b)-ii] Δ_β with synchronous coupling $H=\sin(2\pi\psi)$.

noise $\sigma_1=\sigma_2=\sigma$. The two coupling functions are antiphase: $H=-\sin(2\pi\psi)$ [Fig. 3(b)-i] and synchronous $H=\sin(2\pi\psi)$ [Fig. 3(b)-ii]. The Monte Carlo simulations are the same curves in Fig. 2 in the top two panels. From the asymptotic theory, both the first order in K($c_3=c_4=0$) and the second order in K curves are plotted. The asymptotic theory deviates from the Monte Carlo simulations when noise is relatively large $\sigma=0.15$ (top curves), but is accurate for small noise ($\sigma=0.1$, and $\sigma=0.075$) and coupling values. As expected, the second order theory (dashed-gray) matches better than the first order theory (thin-gray) with small parameters. Notice the first order theory does not depend on σ_2. The first order theory and Monte Carlo simulations are monotonic in K. The second order theory is not monotonic (cf. O-U systems for large σ in Fig. 1), and matches the Monte Carlo simulations better over a larger range of K.

We now consider different noise values where σ_1 is not necessarily equal to σ_2 in the phase models (8) and (9). If $\sigma_1=0$ and $\sigma_2>0$, then coupling naturally increases var(T) of θ_1. Since coupling decreases var(T) when $\sigma_1=\sigma_2$, by continuity we expect there to be a range of $0<\sigma_1<\sigma_2$ where var(T) will still decrease. That is, coupling to a noisier oscillator will still decrease the variability, similar to the diffusively coupled O-U processes analyzed above. The difference here is that we expect this effect to be robust to different types of coupling. This is indeed what is observed in the Monte Carlo simulations (Fig. 4). Formula (10) is not as simple as it appears because coefficients must be determined numerically and they depend in part on the noise and coupling parameters. Thus, it is difficult to make analytic predictions for how disparate the noise levels can be to have coupling decrease variability (cf. O-U processes). Nevertheless, the Monte Carlo simulations and the second order asymptotic theory match quite well (Fig. 4) for the same coupling and PRC in Fig. 3. The first order asymptotic theory ($c_3=c_4=0$) does not depend on σ_2 and is not informative since the variance only decreases in K (thus, it is not plotted in Fig. 4). In Fig. 4, σ_2 is fixed at 0.1, and σ_1 varies between 0 to 0.1. There is a range of $0<\sigma_1<\sigma_2$ values where coupling to a noisier oscillator still decreases variability (e.g., $\sigma_1=0.08$), independent of coupling. The second order asymptotic theory captures these results. The variance of a noisy oscillator similarly decreases when coupled to less noisier oscillator (not shown).

V. REDUCTION IN VARIANCE VIA COUPLING IN FULL OSCILLATOR MODELS

The Morris-Lecar model [24] of giant barnacle muscle behaves as a neural oscillator with large enough input current [Fig. 5(a) shows limit cycle; see Appendix C1 for equations].

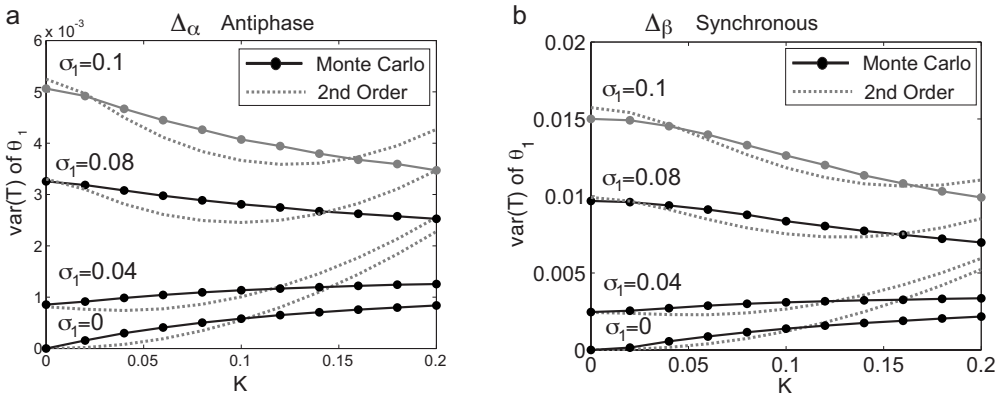

FIG. 4. Comparison of theory and simulations of phase models for $\sigma_1 \neq \sigma_2$ matches well. σ_2 is fixed at 0.1 and σ_1 is varied between 0 to 0.1. (a) For Δ_α with antiphase coupling, var(T) for θ_1 is compared for different K values. (b) Same as (a) except with Δ_β and synchronous coupling. The gray curve is both panels corresponds to when $\sigma_1 = \sigma_2$; it is the same blue curve in Fig. 3(b). The behavior is qualitatively the same as the full oscillator systems in that coupling to a noisier oscillator can decrease the variability.

The density of spike times of an uncoupled noisy cell is plotted in Fig. 5(b) (black). When two Morris-Lecar cells are electrically coupled, the variance of the spike times decreases [Fig. 5(b)]. Notice the interspike-interval (ISI) density becomes narrower (gray and dashed-black) as the coupling strength ($\tilde{K} = g_p$ here) increases. Simulations show that var(T) decreases as coupling increases [Fig. 5(c), top panel] as one would expect from the previous analysis of the reduced phase models. A commonly used dimensionless measure of the variability of T is the coefficient of variation (CV), which is equal to the standard deviation divided by the mean $\mathrm{CV} = \sqrt{\mathrm{var}(T)}/\langle T \rangle$. For example, a Poisson process has mean equal to its standard deviation giving a CV=1, which is highly variable. We see that the CV also decreases with

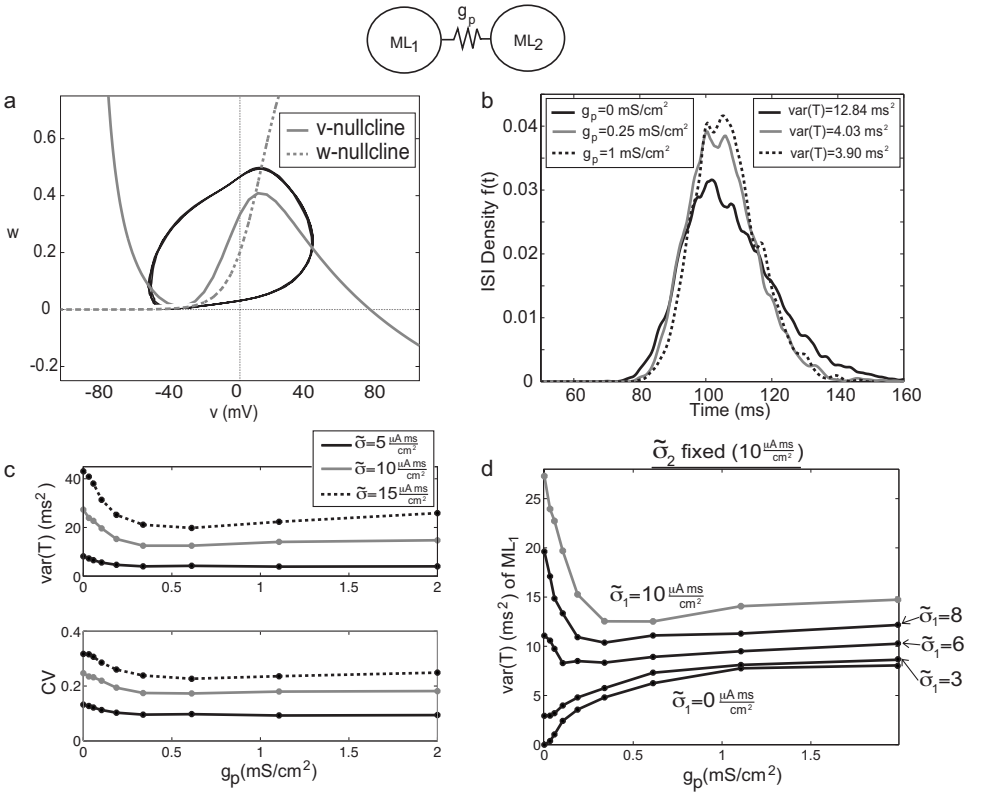

FIG. 5. Reciprocal coupling reduces the variability of spike times of Morris-Lecar model. (a) Morris-Lecar (ML) phase plane with $g_p = 5$ $\frac{\mu A}{cm^2}$ and $\tilde{\sigma}_1 = \tilde{\sigma}_2 = 5$ $\frac{\mu A\ ms}{cm^2}$. (b) Probability density of ISI for various values of electrical coupling $g_p = 0$ (black), 0.25 (gray), and 1 (dashed-black) mS/cm^2 with $\tilde{\sigma}_1 = \tilde{\sigma}_2 = 5$ $\frac{\mu A\ ms}{cm^2}$. (c) The variance and $\mathrm{CV} = \sqrt{\mathrm{var}(T)}/\langle T \rangle$ of the spike times vs. g_p with various noise values ($\tilde{\sigma}_1 = \tilde{\sigma}_2$). The curves are not necessarily monotonic, but coupling always regularizes the ISI compared with the uncoupled system. (d) var(T) of ML$_1$ vs g_p with $\tilde{\sigma}_2 = 10$ $\frac{\mu A\ ms}{cm^2}$ fixed, and $\tilde{\sigma}_1$ varying between 0 to 10 $\frac{\mu A\ ms}{cm^2}$. Notice for $\tilde{\sigma}_1 < \tilde{\sigma}_2$, coupling can *reduce* the variability of the first ML oscillator even though it is coupled to a noisier oscillator ($\tilde{\sigma}_1 = 6, 8$ $\frac{\mu A\ ms}{cm^2}$).

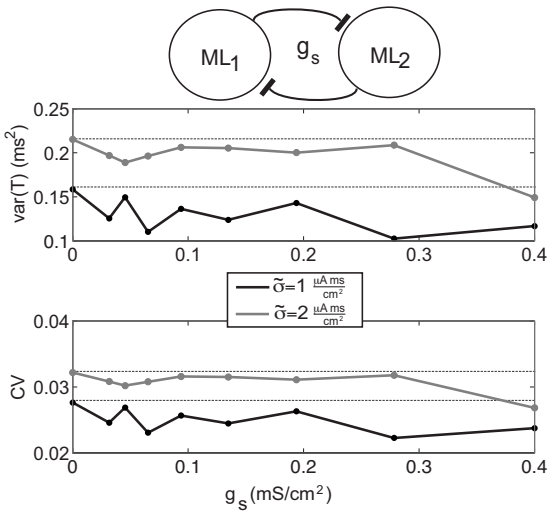

FIG. 6. Morris-Lecar cells coupled via inhibitory synapses. In this absence of noise, the two cells settle to an antiphase state. Synaptic coupling regularizes the spike times of the individual cells. The effect is not dramatic because the noise and coupling parameters have to be quite small for there to be a well-defined phase on the limit cycle. The noise levels are equal and dotted black lines are var(T) for $\tilde{K}=0$.

coupling strength and has a similar shape as the var(T) curve [Fig. 5(c), bottom panel]—this is not surprising because the perturbations are small and the mean $\langle T\rangle$ does not vary much. The CV measure shows the variability is not unreasonably small in light of the small magnitudes of var(T) in the phase models. The variability is not necessarily monotonic in g_p, however, it is evident that any reasonable coupling value regularizes the spike times compared to the uncoupled case. The g_p values in these regimes result in synchronous behavior, which is a well-known effect of electrical coupling in biological cells.

By the same argument as before, for $\tilde{\sigma}_2>0$, we expect a range of $\tilde{\sigma}_1<\tilde{\sigma}_2$ where coupling decreases var(T) of the less noisier oscillator. This is illustrated in Fig. 5(d) shows how coupling to a noisier oscillator can *decrease* the variability. Here $\tilde{\sigma}_2=10$ $\frac{\mu A\ ms}{cm^2}$ is fixed and $\tilde{\sigma}_1$ varies from 0 to 10 $\frac{\mu A\ ms}{cm^2}$. When $\tilde{\sigma}_1=0$ and 3 $\frac{\mu A\ ms}{cm^2}$, the two bottom curves shows how coupling increases the variability of oscillator 1. For intermediate values of $\tilde{\sigma}_1$ (6 and 8 $\frac{\mu A\ ms}{cm^2}$), coupling to the noisier oscillator 2 will decrease the variability. For reference, the curve from Fig. 5(c) where the two oscillators have the same noise value (10 $\frac{\mu A\ ms}{cm^2}$) is plotted in gray. Note that var(T) of the second oscillator also decreases with coupling, even when reciprocally coupled to a less noisier oscillator (not shown). Therefore, this high dimensional system behaves as one would expect given the above results in the reduced phase models.

Next, we consider inhibitory synaptic coupling between the Morris-Lecar cells. The parameters are chosen so that in the absence of noise, the oscillators settle to an antiphase state. Figure 6 shows the synaptic coupling strength g_s can reduce the variability of the spike times, as long as the noise and coupling strengths are small enough (see Appendix C 2 for equations). The values of g_s appear small, but the effective inhibitory current is still significant because it has the form: $g_s s_j(v_i)(v_j-\varepsilon_s)$ [i.e., $(v_j-\varepsilon_s)$ can be >100 mV]. Notice again, the CV is similar to var(T) because mean period does not change much in the asymptotic regime. If the inhibitory synaptic coupling is too strong, var(T) can increase compared to when it is uncoupled. In that case, $\langle T\rangle$ increases and the asymptotic theory (and phase model approximation) are no longer valid.

To test if the results hold in a larger network, we study the statistics of a single Morris-Lecar cell reciprocally coupled to four other Morris-Lecar cells (Fig. 7). The other four cells are not coupled to each other. To properly compare the gap junction strength g_p with Fig. 5, we scale each g_p to $\frac{1}{4}g_p$. From Fig. 7(a), we see that coupling still reduces variability in this network when the noise levels of all the cells are the same. Moreover, if the other four cells are noisier than the first Morris-Lecar cell, coupling will still lower the variability of its spike times of the less noisier oscillator [Fig. 7(b)].

The Brusselator model [25] of oscillating chemical reactions with noise shows the same reduction in variability with diffusive coupling. We focus on two Brusselators, each con-

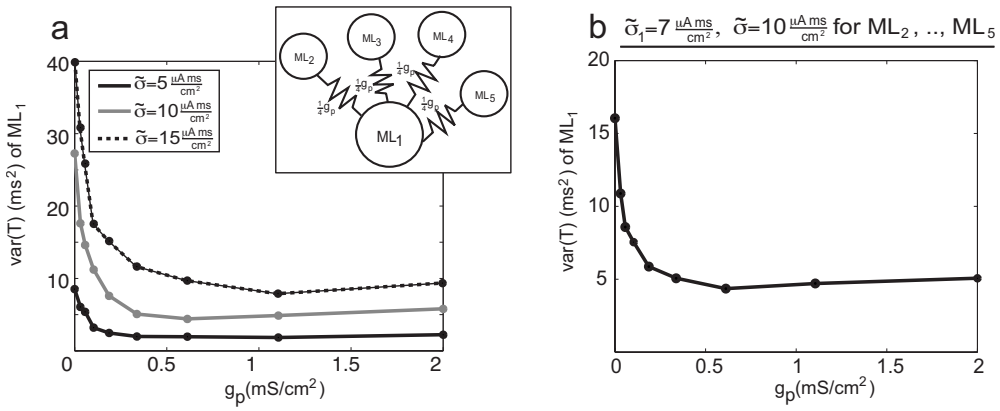

FIG. 7. Coupling reduces variability in a network of Morris-Lecar oscillators. Since ML_1 is coupled to four other MLs, each g_p is scaled to $\frac{1}{4}g_p$ for comparison to Fig. 5. (a) var(T) of a single ML decreases with nonzero g_p. The noise values of each oscillator are the same, with the legend used in Fig. 5(c). (b) The noise of the first ML (7 $\frac{\mu A\ ms}{cm^2}$) is less than the other four MLs (10 $\frac{\mu A\ ms}{cm^2}$), yet coupling still decreases the variance of it's spike times.

sisting of two chemical concentrations (x_j, y_j), $j=1,2$, $x_j \geq 0$, $y_j \geq 0$, that oscillate in the absence of coupling and noise. Assume the y_j's cannot react to each other, the x_j's are diffusively coupled, and they receive random noise perturbations via some background solution.

$$\dot{x}_1 = a - (b+1)x_1 + x_1^2 y_1 - \tilde{K}(x_1 - x_2) + \tilde{\sigma}_1 \xi_1(t),$$

$$\dot{y}_1 = b x_1 - x_1^2 y_1,$$

$$\dot{x}_2 = a - (b+1)x_2 + x_2^2 y_2 - \tilde{K}(x_2 - x_1) + \tilde{\sigma}_2 \xi_2(t),$$

$$\dot{y}_2 = b x_2 - x_2^2 y_2. \tag{11}$$

The parameter values are chosen so that there is a stable limit cycle in the absence of noise and coupling: $b > 1 + a^2$. Here, we choose $a=1$ and $b=3$.

We choose a point of high concentration in y and low concentration in x as the starting point of the limit cycle [Fig. 8(a), gray star]. The decrease in variability of the period with diffusive coupling is not as impressive as with the Morris-Lecar model, but is still evident [Fig. 8(b), with same noise $\tilde{\sigma}_1 = \tilde{\sigma}_2 = \tilde{\sigma}$]. Recall that the variables here are normalized. The noise and coupling parameters are quite small because it does not need a sizable perturbation to deviate far off the limit cycle. Once again, we see range of $\tilde{\sigma}_1 < \tilde{\sigma}_2 = 0.06$ where coupling to a noisier oscillator decreases the variability of the period of the first Brusselator [Fig. 8(c) for $\tilde{\sigma}_1 = 0.045, 0.055$].

VI. DISCUSSION

Many who have studied noisy oscillators have focused on the synchronization properties [18]. Coupling in noisy systems is known to dramatically alter the synchronization properties [18,26]. Also, recent work by Vasseur and Fox [27] suggests that within noisy population dynamics, coupling plays an important role in enabling synchronous behavior in predator-prey systems. We focus on the variability because it is also an important attribute of a system.

Although noise in oscillatory systems can have beneficial consequences [28], it can lead to irregular behavior that is detrimental if precision is required. We have shown that coupling in noisy systems (i.e., diffusively coupled Ornstein-Uhlenbeck processes and nonlinear noisy oscillators) can decrease the variability of the individual units. It is known that population activity can be regularized with coupling [2,6–8,17], often with a reduction in variance proportional to $1/N$ or better [3,4] for large N where N is the population size. *A priori*, it is not obvious why various types of reciprocal coupling with other noisy, possibly noisier, oscillators reduces the variability of a single oscillator. The same coupling-induced regularity is also observed in higher dimensional realistic oscillator models (Morris-Lecar and Brusselator) and in a network setting. We derive an asymptotic theory that captures this phenomenon.

There are parameter regimes in the full systems where coupling can increase the variability of the spike times. In the Morris-Lecar cells with inhibitory synaptic coupling, the oscillator can be held at an inactive state for significant periods of time, increasing the variance compared to the uncoupled system, and increasing the mean time between spikes. This regime is not well approximated by the phase models (8) and (9). However, if the coupling and noise pa-

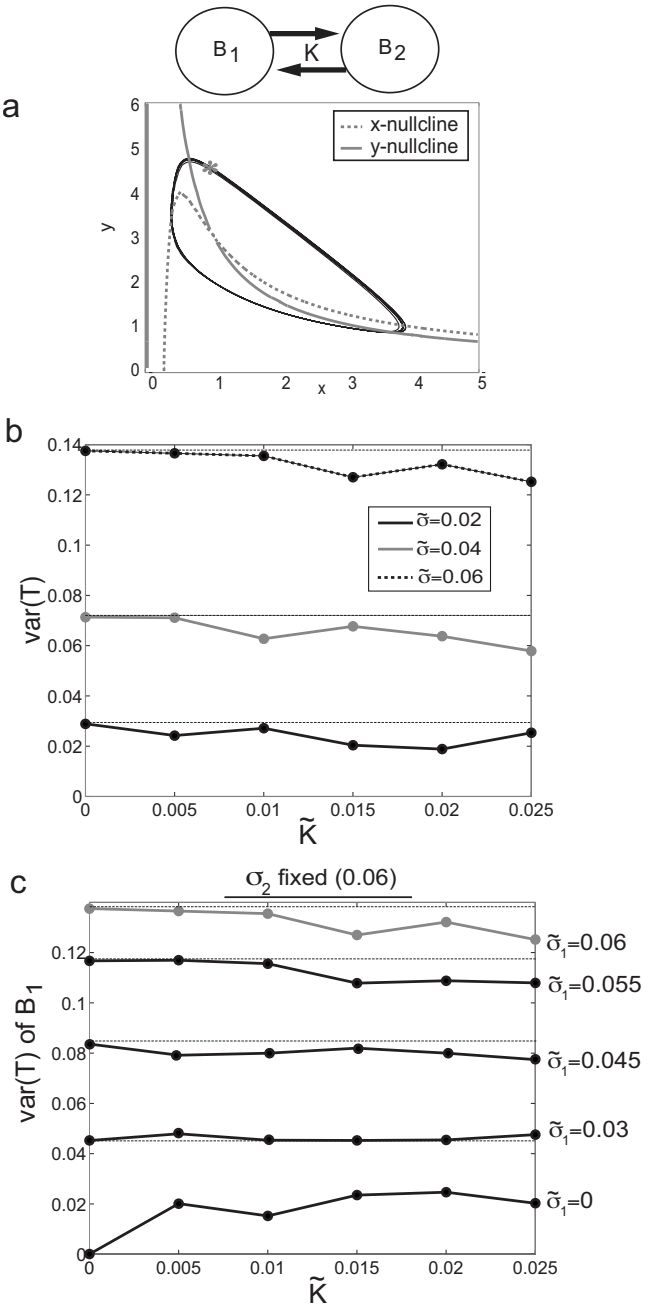

FIG. 8. Brusselator model of oscillating chemical concentrations. (a) Phase plane of concentrations (x_1, y_1) with $\tilde{K}=0.02$, $\tilde{\sigma}=0.05$ for both Brusselators. (b) Variance of period with different coupling strengths $\tilde{K}$ for $\tilde{\sigma}_1 = \tilde{\sigma}_2 = \tilde{\sigma}$. Diffusive coupling regularizes the period of each cycle (dotted black line var(T) for $\tilde{K}=0$). (c) Fixed $\tilde{\sigma}_2=0.06$, variance of period of first Brusselator with different coupling strengths, varying $\tilde{\sigma}_1$ between 0 and 0.06. Again, coupling can *reduce* the variability of the first Brusselator even though it is coupled to a noisier oscillator ($\tilde{\sigma}_1 = 0.045, 0.055$). The gray curve $\tilde{\sigma}_1 = 0.06$ is the top curve in (b) (dashed-black).

rameters are small enough, inhibitory synaptic coupling can slightly regularize the spike times (Fig. 6). Our results hold for general oscillators that are well approximated by the phase models (8) and (9).

The effect of coupling on the regularity of individual oscillators has been addressed briefly (Chapter 9.2.4 in Pikovsky *et al.* [17]) in the specific case where two reciprocally coupled oscillators are synchronized, i.e., the phase difference $\psi \to 0$. Our results are more general than this special limit. In electric fish, reliability across trials of a single neuron was observed by Chacron and co-workers [29]. The trial to trial reliability crucially depended on the entire network being active (i.e., some form of coupling to the single neuron). This is an example of coupling-induced reliability of an individual neuron from trial to trial. This is similar in spirit to our theoretical results, but we show the variability in a single trial is reduced via coupling (for noisy oscillators).

From our results we can make testable experimental predictions in neuroscience. If the interspike-interval (ISI) statistics of a particular uncoupled oscillating neuron are known, then we predict the same type of neuron that is weakly coupled in a network will have more regular ISI. This can be tested in *in vitro* slice preparation. These predictions rely on our specific framework where the coupling and noise strengths are small, and the neurons are repetitively firing action potentials of similar frequencies.

ACKNOWLEDGMENTS

All Monte Carlo simulations for higher dimensional oscillators were smoothed with a Gaussian filter [36]. The simulations were partially aided by computing resources on PittGrid (www.pittgrid.pitt.edu). We thank Brent Doiron for reading the paper and helpful suggestions. Cheng Ly is supported by an NSF Mathematical Sciences Postdoctoral Research Grant No. DMS-0703502. Bard Ermentrout is supported by an NSF Grant No. DMS-0817131.

APPENDIX A: CALCULATION OF ASYMPTOTIC var(T) OF PHASE MODEL

The random trajectory of the two oscillators $\theta_j(t)$ is given by the (Itô) integral equations,

$$\theta_1(t) = t + \sigma_1 \int_0^t \Delta[\theta_1(s)]\xi_1(s)ds + K\int_0^t H[\theta_2(s) - \theta_1(s)] + \frac{\sigma_1^2}{2}\int_0^t \Delta[\theta_1(s)]\Delta'[\theta_1(s)]ds, \tag{A1}$$

$$\theta_2(t) = t + \psi + \sigma_2 \int_0^t \Delta[\theta_2(s)]\xi_2(s)ds + K\int_0^t H[\theta_1(s) - \theta_2(s)]ds + \frac{\sigma_2^2}{2}\int_0^t \Delta[\theta_2(s)]\Delta'[\theta_2(s)]ds, \tag{A2}$$

where we have assumed initial conditions $\theta_1(0)=0$, and $\theta_2(0)=\psi \in (0,1)$ without loss of generality. By periodicity, this is equivalent to having initial phase difference of $\psi \in (0,1)$ (mod 1), where ψ is a random variable with distribution equal to the steady-state density of the phase difference $p(\psi)$. The initial condition does not affect the evolution of the trajectories, so we can proceed with our analysis assuming ψ is fixed. After which, we must average over initial conditions. That is, take the expectation of the resulting formulas over ψ, i.e., replace $g(\psi)$ with $\int_0^1 g(\psi)p(\psi)d\psi$.

Assume the noise strengths σ_j and coupling strength K are small. For notational convenience, let $\xi_j(s)ds = dW_j(s)$. Expanding in powers of σ_1, σ_2, and K, the second term in Eq. (A1), $\sigma_1\int_0^t \Delta[\theta_1(s)]\xi_1(s)ds =$

$$\sigma_1\int_0^t \Delta(s)dW_1(s) + (\sigma_1)^2\int_0^t \Delta'(s)\left[\int_0^s \Delta(r)dW_1(r)\right]dW_1(s) + \sigma_1 KH(\psi)\int_0^t s\Delta'(s)dW_1(s) + h.o.t. \tag{A3}$$

where *h.o.t.* stands for higher order terms. The third term in Eq. (A1) is $K\int_0^t H(\theta_2(s)-\theta_1(s))ds =$

$$KH(\psi)t + K^2H'(\psi)[H(-\psi) - H(\psi)]\frac{t^2}{2} + \sigma_2 KH'(\psi)\int_0^t\left[\int_0^s \Delta(r+\psi)dW_2(r)\right]ds - \sigma_1 KH'(\psi)\int_0^t\left[\int_0^s \Delta(r)dW_1(r)\right]ds + h.o.t. \tag{A4}$$

and the last term in Eq. (A1), $\frac{\sigma_1^2}{2}\int_0^t \Delta[\theta_1(s)]\Delta'[\theta_1(s)]ds$, is simply

$$\frac{\sigma_1^2}{2}\frac{\Delta^2(t)}{2} + h.o.t. \tag{A5}$$

Let us define

$$h_0 := H(\psi), \tag{A6}$$

$$h_p := H'(\psi), \tag{A7}$$

$$\bar{h} := H(-\psi) - H(\psi). \tag{A8}$$

To second order, the random trajectory of $\theta_1(t)$ can be written using Eqs. (A3)–(A5) and Eqs. (A6)–(A8). With random initial condition $\theta_2(0) - \theta_1(0) = \psi$, we have

$$\theta_1(t) = t + \sigma_1 \int_0^t \Delta(s) dW_1(s) + Kh_0 t + (\sigma_1)^2 \left\{ \int_0^t \Delta'(s) \left[\int_0^s \Delta(r) dW_1(r) \right] dW_1(s) + \frac{\Delta^2(t)}{4} \right\} + K^2 h_p \bar{h} \frac{t^2}{2}$$
$$+ \sigma_1 K \left\{ h_0 \int_0^t s\Delta'(s) dW_1(s) - h_p \int_0^t \left[\int_0^s \Delta(r) dW_1(r) \right] ds \right\} + \sigma_2 K h_p \int_0^t \left[\int_0^s \Delta(r+\psi) dW_2(r) \right] ds + h.o.t. \quad \text{(A9)}$$

$$\theta_1(t) = t + \sigma_1 Z_1(t) + KZ_2(t) + (\sigma_1)^2 Z_3(t) + K^2 Z_4(t) + \sigma_1 K Z_5(t) + \sigma_2 K Z_6(t) + h.o.t. \quad \text{(A10)}$$

Note that the functions $Z_j(t)$ are defined as the coefficients of the asymptotic expansion in Eq. (A9). We also expand the random period T in powers of σ_j and K.

$$T = 1 + \sigma_1 T_1 + KT_2 + (\sigma_1)^2 T_3 + K^2 T_4 + \sigma_1 K T_5 + \sigma_2 K T_6 + h.o.t.$$

Substitute $t=T$ into Eq. (A10) and expand the coefficients Z_j as well, keeping in mind $\theta_1(T)=1$ by definition. The result is

$$0 = \sigma_1 T_1 + \sigma_1 [Z_1(1) + Z_1'(1)(\sigma_1 T_1 + KT_2)] + KT_2 + K[Z_2(1) + Z_2'(1)(\sigma_1 T_1 + KT_2)] + (\sigma_1)^2 T_3 + (\sigma_1)^2 Z_3(1) + K^2 T_4 + K^2 Z_4(1) + \sigma_1 K T_5 + \sigma_1 K Z_5(1) + \sigma_2 K[T_6 + Z_6(1)] + h.o.t.$$

Combining like terms, we solve for T_j by making the coefficients of noise and coupling vanish, term by term

$$T_1 = -Z_1(1),$$

$$T_2 = -Z_2(1),$$

$$T_3 = -Z_3(1) - Z_1'(1)T_1,$$

$$T_4 = -Z_4(1) - Z_2'(1)T_2,$$

$$T_5 = -Z_5(1) - Z_1'(1)T_2 - Z_2'(1)T_1,$$

$$T_6 = -Z_6(1).$$

The expanded expressions for T_j are

$$T_1 = -\int_0^1 \Delta(s) dW_1(s), \quad \text{(A11)}$$

$$T_2 = -h_0, \quad \text{(A12)}$$

$$T_3 = -\int_0^1 \Delta'(s) \left[\int_0^s \Delta(r) dW_1(r) \right] dW_1(s), \quad \text{(A13)}$$

$$T_4 = -h_p \frac{\bar{h}}{2} + h_0^2, \quad \text{(A14)}$$

$$T_5 = h_p \int_0^1 \left[\int_0^s \Delta(r) dW_1(r) \right] ds + h_0 \int_0^1 [\Delta(s) - s\Delta'(s)] dW_1(s), \quad \text{(A15)}$$

$$T_6 = -h_p \int_0^1 \left[\int_0^s \Delta(r+\psi) dW_2(r) \right] ds. \quad \text{(A16)}$$

We can now compute the statistics of

$$T = 1 + \sigma_1 T_1 + KT_2 + (\sigma_1)^2 T_3 + K^2 T_4 + \sigma_1 K T_5 + \sigma_2 K T_6$$

to second order. The mean of T is

$$\langle T \rangle = 1 - Kh_0 + K^2 \left(-h_p \frac{\bar{h}}{2} + h_0^2 \right). \quad \text{(A17)}$$

Note that $\langle T_3 \rangle = -\int_0^1 \Delta'(s)\Delta(s) ds = \int_0^1 \Delta'(s)\Delta(s) ds = 0$. The variance of T, $\mathrm{var}(T) = \langle (T - \langle T \rangle)^2 \rangle$, is

$$\mathrm{var}(T) = \langle (\sigma_1 T_1 + (\sigma_1)^2 T_3 + \sigma_1 K T_5 + \sigma_2 K T_6)^2 \rangle. \quad \text{(A18)}$$

Many of the terms vanish in the $\mathrm{var}(T)$ calculation because the noise in θ_1 and θ_2 are independent $\langle dW_1 \cdot dW_2 \rangle = 0$, and odd powers of noise have expectation $0: \sigma_j^{2k+1} \langle dW_j \cdot dW_j \ldots dW_j \rangle = 0$. We simplify Eq. (A18) to

$$\mathrm{var}(T) = (\sigma_1)^2 \langle T_1^2 \rangle + 2(\sigma_1)^2 K \langle T_1 T_5 \rangle + (\sigma_1 K)^2 \langle T_5^2 \rangle + (\sigma_2 K)^2 \langle T_6^2 \rangle + (\sigma_1)^4 \langle T_3^2 \rangle. \quad \text{(A19)}$$

The covariances of T_j of interest are

$$\langle T_1^2 \rangle = \int_0^1 \Delta^2(s) ds, \quad \text{(A20)}$$

$$\langle T_1 T_5 \rangle = -h_p \int_0^1 (1-s)\Delta^2(s) ds + h_0 \int_0^1 s\Delta'(s)\Delta(s) - \Delta^2(s) ds, \quad \text{(A21)}$$

$$\langle T_5^2 \rangle = (h_p)^2 \left[\int_0^1 \int_0^s \int_0^{s'} \Delta^2(r) dr ds' ds + \int_0^1 (1-s) \int_0^s \Delta^2(r) dr ds \right] + 2h_0 h_p \int_0^1 (1-s)\Delta^2(s) - (1-s)s\Delta(s)\Delta'(s) ds$$

TABLE I. Various definite integral values [see definitions in Eq. (A25)]. For canonical type II $\Delta_\alpha=-\sin(2\pi\theta)$ and type I $\Delta_\beta=1-\cos(2\pi\theta)$ PRCs.

Definite Integral	Type II Δ_α	Type I Δ_β
L_0	$\frac{1}{2}$	$\frac{3}{2}$
L_1	$\frac{1}{4}$	$\frac{3}{4}$
$\int_0^1\int_0^s\int_0^{s'}\Delta^2(r)drds'ds+\int_0^1(1-s)\int_0^s\Delta^2(r)drds$	$\frac{1}{6}-\frac{1}{16\pi^2}$	$\frac{1}{2}-\frac{15}{16\pi^2}$
$\int_0^1\int_0^s\int_0^{s'}\Delta^2(r+\psi)drds'ds+\int_0^1(1-s)\int_0^s\Delta^2(r+\psi)drds$	$\frac{1}{6}-\frac{1}{16\pi^2}+\frac{\cos^2(\pi\psi)}{2\pi^2}-\frac{\cos^4(\pi\psi)}{2\pi^2}-\frac{\sin(2\pi\psi)}{4\pi}+\frac{\cos^3(\pi\psi)\sin(\pi\psi)}{\pi}$	$\frac{1}{2}+\frac{17}{16\pi^2}-\frac{5\cos^2(\pi\psi)}{2\pi^2}+\frac{\cos^4(\pi\psi)}{2\pi^2}+\frac{5\sin(2\pi\psi)}{4\pi}-\frac{\cos^3(\pi\psi)\sin(\pi\psi)}{\pi}$
$\int_0^1 s^2(\Delta'(s))^2ds$	$\frac{2}{3}\pi^2+\frac{1}{4}$	$\frac{2}{3}\pi^2-\frac{1}{4}$
$\frac{1}{2}\int_0^1[\Delta'(s)]^2\int_0^s\Delta^2(r)drds$	$\frac{1}{4}\pi^2$	$\frac{3}{4}\pi^2$

$$+(h_0)^2\left\{\int_0^1\Delta^2(s)-2s\Delta(s)\Delta'(s)+s^2[\Delta'(s)]^2ds\right\} \tag{A22}$$

$$\langle T_6^2\rangle=h_p^2\left[\int_0^1\int_0^s\int_0^{s'}\Delta^2(r+\psi)drds'ds+\int_0^1(1-s)\int_0^s\Delta^2(r+\psi)drds\right], \tag{A23}$$

$$\langle T_3^2\rangle=\frac{1}{2}\int_0^1[\Delta'(s)]^2\int_0^s\Delta^2(r)drds. \tag{A24}$$

For convenience, let us define

$$L_0=\int_0^1\Delta^2(s)ds, \tag{A25}$$

$$L_1=\int_0^1 s\Delta^2(s)ds, \tag{A26}$$

$$L_2=\int_0^1 s^2\Delta^2(s)ds. \tag{A27}$$

The terms above can be partially simplified by integrating by parts

$$\int_0^1 s\Delta(s)\Delta'(s)ds=-\frac{1}{2}L_0,$$

$$\int_0^1 s^2\Delta(s)\Delta'(s)ds=-L_1.$$

In terms of the L's, we have

$$\langle T_1^2\rangle=L_0, \tag{A28}$$

$$\langle T_1T_5\rangle=-h_p(L_0-L_1)-\frac{3}{2}h_0L_0, \tag{A29}$$

$$\langle T_5^2\rangle=(h_p)^2\left[\int_0^1\int_0^s\int_0^{s'}\Delta^2(r)drds'ds+\int_0^1(1-s)\int_0^s\Delta^2(r)drds\right]+h_0h_p(3L_0-4L_1)+(h_0)^2\left\{2L_0+\int_0^1 s^2[\Delta'(s)]^2ds\right\}, \tag{A30}$$

$$\langle T_6^2\rangle=h_p^2\left[\int_0^1\int_0^s\int_0^{s'}\Delta^2(r+\psi)drds'ds+\int_0^1(1-s)\int_0^s\Delta^2(r+\psi)drds\right], \tag{A31}$$

$$\langle T_3^2\rangle=\frac{1}{2}\int_0^1[\Delta'(s)]^2\int_0^s\Delta^2(r)drds. \tag{A32}$$

These terms can be calculated for a specific Δ (see Table I). For type II $\Delta_\alpha=-\sin(2\pi\phi)$, the values are [recall Eqs. (A6) and (A7)],

$$\langle T_1^2\rangle = \frac{1}{2},$$

$$\langle T_1 T_5\rangle = -\frac{1}{4}[H'(\psi) + 3H(\psi)],$$

$$\langle T_5^2\rangle = (H'(\psi))^2\left(\frac{1}{6} - \frac{1}{16\pi^2}\right) + \frac{1}{2}H(\psi)H'(\psi) + H(\psi)^2\left(\frac{5}{4} + \frac{2}{3}\pi^2\right),$$

$$\langle T_6^2\rangle = (H'(\psi))^2\left(\frac{1}{6} + \ldots(\text{see Table I, fourth row})\right),$$

$$\langle T_3^2\rangle = \frac{1}{4}\pi^2,$$

and for type I $\Delta_\beta = 1-\cos(2\pi\phi)$,

$$\langle T_1^2\rangle = \frac{3}{2},$$

$$\langle T_1 T_5\rangle = -\frac{3}{4}[H'(\psi) + 3H(\psi)],$$

$$\langle T_5^2\rangle = (H'(\psi))^2\left(\frac{1}{2} - \frac{15}{16\pi^2}\right) + \frac{3}{2}H(\psi)H'(\psi) + H(\psi)^2\left(\frac{11}{4} + \frac{2}{3}\pi^2\right),$$

$$\langle T_6^2\rangle = [H'(\psi)]^2\left[\frac{1}{2} + \ldots(\text{see Table I, fourth row})\right],$$

$$\langle T_3^2\rangle = \frac{3}{4}\pi^2.$$

These coefficients are then averaged over initial conditions: $\int_0^1 \langle T_i T_j\rangle p(\psi)d\psi$ to complete the formula for var(T) in Eq. (A19),

$$\text{var}(T) = c_1(\sigma_1)^2 + c_2(\sigma_1)^2 K + c_3(\sigma_1 K)^2 + c_4(\sigma_2 K)^2 + c_5(\sigma_1)^2, \tag{A33}$$

$$c_1 = \langle T_1^2\rangle, \tag{A34}$$

$$c_2 = 2\int_0^1 \langle T_1 T_5\rangle p(\psi)d\psi, \tag{A35}$$

$$c_3 = \int_0^1 \langle T_5^2\rangle p(\psi)d\psi, \tag{A36}$$

$$c_4 = \int_0^1 \langle T_6^2\rangle p(\psi)d\psi, \tag{A37}$$

$$c_5 = \langle T_3^2\rangle. \tag{A38}$$

APPENDIX B: STATISTICAL QUANTITIES OF PHASE MODEL VIA THE FOKKER-PLANCK EQUATION

Statistical quantities of event times (e.g., spikes) can be computed via a modification of the Fokker-Planck equation [23]. Although there are other methods to obtain these statistical quantities (see Touboul and Faugeras [30] for some techniques), they generally require nontrivial numerical methods when the system is high dimensional. We focus on how to obtain these quantities via the Fokker-Planck equation.

Recall the Itô SDEs for the reduced phase model (8) and (9),

$$\dot\theta_1 = 1 + KH(\theta_2 - \theta_1) + \frac{\sigma_1^2}{2}\Delta(\theta_1)\Delta'(\theta_1) + \sigma_1\Delta(\theta_1)\xi_1(t),$$

$$\dot\theta_2 = 1 + KH(\theta_1 - \theta_2) + \frac{\sigma_2^2}{2}\Delta(\theta_2)\Delta'(\theta_2) + \sigma_2\Delta(\theta_2)\xi_2(t). \tag{B1}$$

The evolution equation for the two-dimensional (2D) probability density $\rho(\theta_1,\theta_2,t)$ is governed by a Fokker-Planck equation [23],

$$\begin{aligned}\frac{\partial\rho}{\partial t} &= -\frac{\partial}{\partial\theta_1}\left\{\left[1 + KH(\theta_2-\theta_1) + \frac{\sigma_1^2}{2}\Delta(\theta_1)\Delta'(\theta_1)\right]\rho\right\} \\ &+ \frac{\sigma_1^2}{2}\frac{\partial^2}{\partial\theta_1^2}[\Delta^2(\theta_1)\rho] \\ &- \frac{\partial}{\partial\theta_2}\left\{\left[1 + KH(\theta_1-\theta_2) + \frac{\sigma_2^2}{2}\Delta(\theta_2)\Delta'(\theta_2)\right]\rho\right\} \\ &+ \frac{\sigma_2^2}{2}\frac{\partial^2}{\partial\theta_2^2}[\Delta^2(\theta_2)\rho] + \delta(\theta_1)([1 + KH(\theta_2 - 1)]\rho(1,\theta_2,t)) \\ &+ \delta(\theta_2)([1 + KH(\theta_1 - 1)]\rho(\theta_1,1,t)).\end{aligned} \tag{B2}$$

Let us call the probability density for the random times $\theta_1(T)=1$ [with $\theta_1(0)=0$] the ISI (interspike-interval) density $f(t)$. The density $f(t)$ can be obtained with Eq. (B2) by removing the reset condition in θ_1: $\delta(\theta_1)([1+KH(\theta_2-1)]\rho(1,\theta_2,t))$, make $\theta_1=1$ an absorbing boundary, and setting the initial condition to

$$\rho(\theta_1,\theta_2,0) = \delta(\theta_1)c\rho_\infty(1,\theta_2),$$

where ρ_∞ is the steady-state density ($\frac{\partial\rho}{\partial t}=0$) of Eq. (B2), and

$$c = \left[\int_0^1 \rho_\infty(1,\theta_2)d\theta_2\right]^{-1}$$

so that the initial probability mass is 1. The ISI density is the flux across $\theta_1=1$,

$$f(t) = \int_0^1 [1 + KH(\theta_2 - 1)]\rho(1, \theta_2, t)d\theta_2. \quad \text{(B3)}$$

See Cox, Lewis, Perkel and co-workers [31–33] for similar equations for spike train statistics. We see $\lim_{t\to\infty} f(t)=0$ because of the absorbing boundary at $\theta_1=1$, and $\int_0^\infty f(t)dt=1$ because the total probability mass absorbed at $\theta_1=1$ is equal to the initial probability mass (i.e., 1). From this, we can obtain the ISI statistics: $\langle T\rangle=\int_0^\infty tf(t)dt$ and $\mathrm{var}(T)=\int_0^\infty t^2 f(t)dt-\langle T\rangle^2$. Solving for the ISI density $f(t)$ numerically is difficult because it not only involves a 2D partial differential equation, but the initial density has a δ-function component that results in instabilities with standard numerical methods. The ISI density of an excitatory leaky integrate-and-fire spiking neuron was solved using a modified finite volume method that relied on analytic formulas for the time steps [34]; however, this is a difficult task for a given Fokker-Planck equation.

The autocorrelation function of θ_1, $A(t-t')=E[\theta_1(t)=1 \,|\, \theta_1(t')=1]$, could be obtained by solving the same equation with the same initial density above but with the reset term $\delta(\theta_1)$ so that probability is conserved (see Peskin [35]). We then have,

$A(t)=\int_0^1[1+KH(\theta_2-1)]\rho(1,\theta_2,t)d\theta_2$. This will give the single-sided autocorrelation function $t-t'\geq 0$; since the process is stationary: $A(t)=A(-t)$. The cross-correlation function, $C(t-t')=E[\theta_1(t)=1 \,|\, \theta_2(t')=1]$, is the flux through θ_1 with the same equation with reset in both θ_1 and θ_2, but with initial density: $\rho(\theta_1,\theta_2,0)=\delta(\theta_2)\hat{c}\rho_\infty(\theta_1,1)$, where $\hat{c}=[\int_0^1\rho_\infty(\theta_1,1)d\theta_1]^{-1}$, and again ρ_∞ is the steady-state density of Eq. (B2).

APPENDIX C: MORRIS-LECAR EQUATIONS

1. Gap junction coupling

The equations of two Morris-Lecar model of a giant barnacle muscle with noise, coupled via gap junctions consists of voltage $v_j(t)$ and an inactivating variable (potassium, etc.) $w_j(t)$,

$$C\dot{v}_1 = I_{app} - g_l\cdot(v_1-\varepsilon_l) - g_k w_1(v_1)(v_1-\varepsilon_k) - g_{ca}m_\infty(v_1)(v_1-\varepsilon_{ca}) - g_p(v_1-v_2) + \tilde{\sigma}_1\xi_1(t),$$

$$\dot{w}_2 = \varphi\frac{w_\infty(v_1)-w_1(v_1)}{\tau_w(v_1)},$$

$$C\dot{v}_2 = I_{app} - g_l\cdot(v_2-\varepsilon_l) - g_k w_2(v_2)(v_2-\varepsilon_k) - g_{ca}m_\infty(v_1)(v_1-\varepsilon_{ca}) - g_p(v_2-v_1) + \tilde{\sigma}_2\xi_2(t),$$

$$\dot{w}_2 = \varphi\frac{w_\infty(v_2)-w_2(v_2)}{\tau_w(v_2)}, \quad \text{(C1)}$$

with $\langle\xi_j(t)\rangle=0$, and $\langle\xi_j(t)\xi_i(t)\rangle=\delta_{ij}\delta(t-t')$. The auxiliary functions are

$$m_\infty(v) = 0.5\{1+\tanh[(v-v_a)/v_b]\},$$

$$w_\infty(v) = 0.5\{1+\tanh[(v-v_c)/v_d]\},$$

$$\tau_w(v) = \frac{1}{\cosh[(v-v_c)/(2v_d)]},$$

The fixed parameter values are: $C=20\ \frac{\mu F}{cm^2}$, $I_{app}=40\ \frac{\mu A}{cm^2}$, $g_l=2\ \frac{mS}{cm^2}$, $\varepsilon_l=-60$ mV, $g_k=8\ \frac{mS}{cm^2}$, $\varepsilon_k=-84$ mV, $g_{ca}=4\ \frac{mS}{cm^2}$, $\varepsilon_{ca}=120$ mV, $g_p=0.01\ \frac{mS}{cm^2}$. For the auxiliary functions: $v_a=-1.2$ mV, $v_b=18$ mV, $v_c=12$ mV, $v_d=17.4$ mV, $\varphi=\frac{1}{15}\ \mathrm{ms}^{-1}$.

2. Inhibitory synaptic coupling

With inhibitory synapses, the Morris-Lecar equations are

$$C\frac{dv_1}{dt} = I_{app} - g_l(v_1-\varepsilon_l) - g_k w_1(v_1)(v_1-\varepsilon_k) - g_{ca}m_\infty(v_1)(v_1-\varepsilon_{ca}) - g_s s_1(v_2)(v_1-\varepsilon_s) + \tilde{\sigma}\xi_1(t),$$

$$\frac{dw_1}{dt} = \varphi\frac{w_\infty(v_1)-w_1(v_1)}{\tau_w(v_1)},$$

$$C\frac{dv_2}{dt} = I_{app} - g_l(v_2-\varepsilon_l) - g_k w_2(v_2)(v_2-\varepsilon_k) - g_{ca}m_\infty(v_1)(v_1-\varepsilon_{ca}) - g_s s_2(v_1)(v_2-\varepsilon_s) + \tilde{\sigma}\xi_2(t),$$

$$\frac{dw_2}{dt} = \varphi\frac{w_\infty(v_2)-w_2(v_2)}{\tau_w(v_2)},$$

$$\frac{ds_i}{dt} = \varphi_s\frac{s_\infty(v_j)-s_i(v_j)}{\tau_s(v_j)}, \quad i=1 \text{ or } 2, \text{ and } i\neq j, \quad \text{(C2)}$$

with $\langle\xi_j(t)\rangle=0$, and $\langle\xi_j(t)\xi_i(t)\rangle=\delta_{ij}\delta(t-t')$. The auxiliary functions are

$$m_\infty(v) = 0.5\{1+\tanh[(v-v_a)/v_b]\}$$

$$w_\infty(v) = 0.5\{1+\tanh[(v-v_c)/v_d]\}$$

$$s_\infty(v) = \frac{\alpha}{\alpha+\beta(1+e^{-(v-v_t)/v_s})},$$

$$\tau_w(v) = \frac{1}{\cosh[(v-v_c)/(2v_d)]},$$

$$\tau_s(v) = \frac{1+e^{-(v-v_t)/v_s}}{\beta\cdot(1+e^{-(v-v_t)/v_s})+\alpha}. \quad \text{(C3)}$$

The parameter values in Fig. 6 are: $C=20\ \frac{\mu F}{cm^2}$, $I_{app}=48\ \frac{\mu A}{cm^2}$, $g_l=2\ \frac{mS}{cm^2}$, $\varepsilon_l=-60$ mV, $g_k=8\ \frac{mS}{cm^2}$, $\varepsilon_k=-84$ mV, $g_{ca}=4\ \frac{mS}{cm^2}$, $\varepsilon_{ca}=120$ mV, $\varepsilon_s=-84$ mV, $\tilde{\sigma}=1.632$. For the auxiliary functions: $v_a=-1.2$ mV, $v_b=18$ mV, $v_c=12$ mV, $v_d=17.4$ mV, $\varphi=\frac{1}{15}\ \mathrm{ms}^{-1}$, $v_t=48$ mV, $v_s=0.05$ mV, $\alpha=1$, $\beta=2$, $\varphi_s=1\ \mathrm{ms}^{-1}$.

[1] P. Tiesinga, J. Fellous, and T. Sejnowski, Nat. Rev. Neurosci. **9**, 97 (2008).
[2] D. Mar, C. Chow, W. Gerstner, R. Adams, and J. Collins, Proc. Natl. Acad. Sci. U.S.A. **96**, 10450 (1999).
[3] M. Spiridon and W. Gerstner, Network **10**, 257 (1999).
[4] P. Tiesinga and T. Sejnowski, Network **12**, 215 (2001).
[5] D. Needleman, P. Tiesinga, and T. Sejnowski, Physica D **155**, 324 (2001).
[6] A. Sherman, J. Rinzel, and J. Keizer, Biophys. J. **54**, 411 (1988).
[7] J. Clay and R. DeHann, Biophys. J. **28**, 377 (1979).
[8] J. Vilar, H. Kueh, N. Barkai, and S. Leibler, Proc. Natl. Acad. Sci. U.S.A. **99**, 5988 (2002).
[9] S. Hughes, M. Lörincz, D. Cope, K. Blethyn, K. Kékesi, H. Parri, G. Juhász, and V. Crunelli, Neuron **42**, 253 (2004).
[10] D. DiFrancesco, Annu. Rev. Physiol. **55**, 455 (1993).
[11] S. Grillner, Neuron **52**, 751 (2006).
[12] S. Jadhav, J. Wolfe, and D. Feldman, Nat. Neurosci. **12**, 792 (2009).
[13] T. Hromádka, M. DeWeese, and A. Zador, PLoS Biol. **6**, e16 (2008).
[14] Y. Kuramoto, *Chemical Oscillations, Waves and Turbulence* (Springer-Verlag, New York, 1984).
[15] A. T. Winfree, J. Math. Biol. **1**, 73 (1974).
[16] J. A. Acebrón, L. L. Bonilla, C. J. Pérez Vicente, F. Ritort, and R. Spigler, Rev. Mod. Phys. **77**, 137 (2005).
[17] A. Pikovsky, M. Rosenblum, and J. Kurths, *Synchronization: A Universal Concept in Nonlinear Sciences* (Cambridge University Press, Cambridge, England, 2001).
[18] C. Zhou and J. Kurths, Phys. Rev. Lett. **88**, 230602 (2002); J. N. Teramae and D. Tanaka, *ibid.* **93**, 204103 (2004); R. F. Galán, G. B. Ermentrout, and N. N. Urban, *ibid.* **94**, 158101 (2005); H. Nakao, K. Arai, and Y. Kawamura, *ibid.* **98**, 184101 (2007); S. Marella and G. B. Ermentrout, Phys. Rev. E **77**, 041918 (2008); C. Ly and G. B. Ermentrout, J. Comput. Neurosci. **26**, 425 (2009).
[19] R. Stratonovich, SIAM J. Control **4**, 362 (1966).
[20] E. Wong and M. Zakai, Probab. Theory Relat. Fields **12**, 87 (1969).
[21] J. N. Teramae, H. Nakao, and G. B. Ermentrout, Phys. Rev. Lett. **102**, 194102 (2009).
[22] G. B. Ermentrout, Neural Comput. **8**, 979 (1996).
[23] H. Risken, *The Fokker-Planck Equation: Methods of Solution and Applications* (Springer-Verlag, Berlin, 1989).
[24] C. Morris and H. Lecar, Biophys. J. **35**, 193 (1981).
[25] I. Prigogine and G. Nicolis, J. Chem. Phys. **46**, 3542 (1967).
[26] M. G. Rosenblum, A. S. Pikovsky, and J. Kurths, Phys. Rev. Lett. **76**, 1804 (1996).
[27] D. Vasseur and J. Fox, Nature (London) **460**, 1007 (2009).
[28] G. B. Ermentrout, R. Galán, and N. Urban, Trends Neurosci. **31**, 428 (2008).
[29] M. Chacron, B. Doiron, L. Maler, A. Longtin, and J. Bastian, Nature (London) **423**, 77 (2003).
[30] J. Touboul and O. Faugeras, J. Physiol. Paris **101**, 78 (2007).
[31] D. R. Cox, *Renewal Theory* (Wiley, New York, 1962).
[32] D. Cox and P. Lewis, *The Statistical Analysis of Series of Events* (Mathuen, London, 1966).
[33] D. Perkel, G. Gerstein, and G. Moore, J. Biophys. **7**, 391 (1967).
[34] C. Ly and D. Tranchina, Neural Comput. **21**, 360 (2009).
[35] C. Peskin, in *Mathematical Aspects of Physiology*, edited by F. C. Hoppensteadt (American Mathematical Society, Providence, RI, 1981), Vol. 19, pp. 59–67.
[36] T. O'Haver, MATLAB Central File Exchange http://www.mathworks.com/matlabcentral/fileexchange/19998 (2008).